

11th International Conference

1-3 July 2013

Pisa



A REVIEW OF A FATIGUE FAILURE WITH AN AIRCRAFT ENGINE NACELLE BULKHEAD

David M.A. Millar^{1*}, Neil S. Ferguson²

¹ Senior Staff Engineer
Bombardier Aerospace Belfast
Airport Road, Belfast, BT3 9DZ, Northern Ireland
E-mail: david.m.millar@aero.bombardier.com

² Engineering and the Environment
University of Southampton
Highfield, Southampton, SO17 1BJ, United Kingdom
E-mail: nsf@isvr.soton.ac.uk

Keywords: Nacelle, acoustic fatigue, dynamic stiffness.

ABSTRACT

The paper discusses some of the fatigue problems observed in-service with components on aircraft engine nacelles. Acoustic fatigue (or sonic fatigue) has been an issue with nacelle components given the proximity of the structure to the high intensity noise generated by the fan on modern high bypass ratio gas turbine aircraft engines.

Reference is made to test measurements – both full scale engine testing and sub-element component testing. Theoretical result predictions using finite element models are summarised and compared with the test measurements. The dynamic stiffness method is also used to predict the fundamental frequency and strain response and shows good agreement with test data.

1. INTRODUCTION

A view of typical jet engine nacelle has been shown in Figure 1.



Figure 1 – Aircraft engine nacelle.

The leading edge of the nacelle is called the lipskin. As shown in Figure 2, a closed cell is formed by attaching a bulkhead (the forward bulkhead) to the lipskin. The purpose of this cell is to contain the thermal anti-ice (TAI) air which is distributed around the circumference of the lipskin by a spray ring. The cell also provides some torsional rigidity and helps support the outer skin of the nacelle. The forward bulkhead is the main focus of attention in this paper as several different configurations have exhibited failure of the web and outer boundary angle. An example of the type of damage typically observed is shown in Figure 3 for reference.

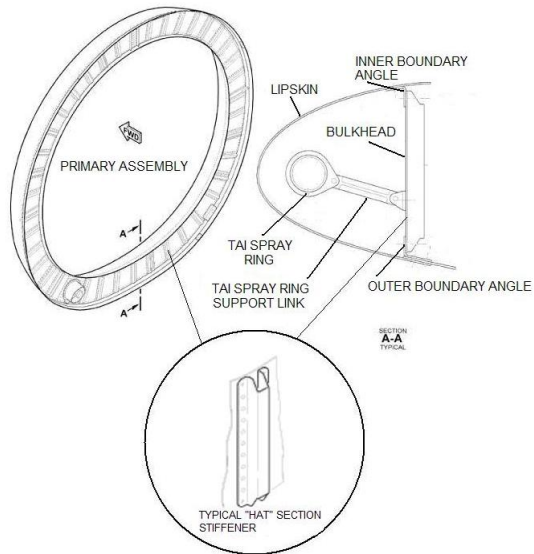


Figure 2 – Primary assembly constituent parts.



Figure 3 – Typical bulkhead damage observed.

2. GENERAL DISCUSSION

As stated previously, several nacelle applications have experienced bulkhead problems of the nature shown in Figure 3; namely cracked bulkhead webs and cracked outer boundary angles. The form of construction of the bulkheads were generally the same in the sense that all had webs made from commercially pure titanium¹ (CP-Ti) and outer boundary angles made from aluminium alloy 2219-T62. The web thickness was typically in the range of 0.64mm to 0.71mm (0.025" to 0.028") while the boundary angles were in the 1.0mm to 1.6mm (0.04" to 0.063") range depending on the attachment configuration². The bulkheads webs were all stiffened by radially aligned stiffeners (generally of the "top-hat" configuration) – these were all formed using 1.0mm (0.04") CP-Ti however, the stiffener spacing varied depending upon nacelle configuration.

The nacelle components are generally considered to be lightly loaded under normal operation. The design conditions are generally associated with failure conditions of other components such as the loss of a fan blade or the failure of an anti-ice duct exposing the surrounding structure to high pressure and temperature. Under normal operation vibration loads and acoustic loading produce high cycle fatigue cases which must also be considered.

2.1 Acoustic fatigue

Acoustic fatigue began to emerge during the 1950's with the advent of the more widespread use of jet engines with commercial aircraft in particular. The work by Miles [1] laid down the basic approach to acoustic fatigue calculations and is the basis used in various design guides [2, 3]. Powell [4] provided a more general treatment of the subject and introduced the concept of joint acceptance which is used to estimate the efficiency with which the sound field can couple with the structural modes of vibration. Blevins [5] proposed assuming a pressure distribution that essentially equates to having a joint acceptance of unity and is a method that is extremely efficient for finite element analysis. A good source for general background on the subject was compiled by Clarkson [6] however, in terms of specific work relating to nacelles there is very little published literature. Holehouse [7] and Soovere [8] discuss problems with nacelle intake barrels in particular and although Holehouse [7] does allude to bulkhead boundary angle problems, no extensive details are reported. In more recent times nacelles have been the subject of work by Millar [9] and Cunningham [10], however again the main subject area was sandwich panels. Work by Millar [11] discusses problems with both sandwich panels and stiffened panels and this has formed the basis for much of the data within this publication.

3. PROCEDURE FOR PROBLEM RESOLUTION

Historically an argument was made at certification that the forward bulkhead in particular, because it was not directly exposed to the fan and was located a distance from the fan behind a noise attenuating panel, that it would not be susceptible to acoustic fatigue. With the advent of failures in the field, this was clearly not the case. The approach adopted to resolve such cases involved a combination of both testing and analysis. In the case of the component being considered here, the testing comprised a progressive wave tube (PWT) test to establish the endurance of the component and also a series of ground engine running tests and flight tests involving a bulkhead which had been instrumented with strain gauges and accelerometers. Parts of the nacelle also had pressure transducers to measure the sound pressure levels generated by the engine. Knowing the typical "normal operating" environment enabled the

¹ The specific grade of commercially pure titanium was AMS4901.

² Some boundary angle attachments employed the use of a single formed angle while others used "back-to-back" angles with the web sandwiched between the two angles.

endurance test in the PWT to indicate the margin expected of the actual structure. The test data also enabled the finite element model to be validated and as such, gave a degree of confidence that the FE model could give an accurate prediction for the response of the proposed solution configuration.

3.1 Progressive wave tube testing

Due to the layout of the nacelle, the forward bulkhead is deeper at the bottom (power plant radial; PPR 180°) than it is at the top (PPR 0°). This results in bays being of different size (Figure 4).

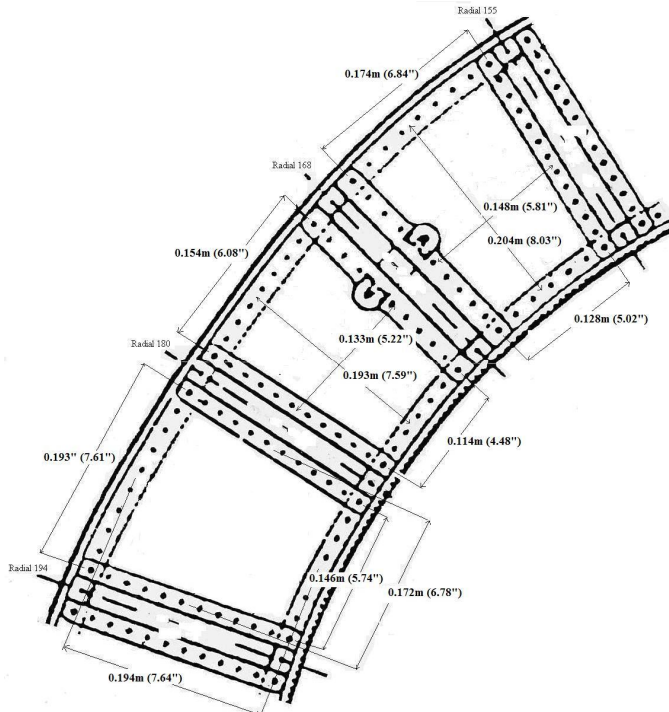


Figure 4 - Bulkhead PWT specimen (Titanium web and stiffeners; overall panel dimensions in inches as shown. Web thickness was 0.7112mm).

A view of the PWT facility at the University of Southampton is shown in Figure 5. The aperture for the test specimen is approximately 1.2m x 0.6m (48" x 24"). The mean diameter of the actual bulkhead is approximately 1.8m (70"); clearly it is not feasible to fit an entire bulkhead into a typical PWT. In the case of a bulkhead, it is usually possible to accommodate a specimen of several bays. In this case, the test specimen incorporated three bays, of which the central bay had the most realistic boundary conditions. The specimen was chosen from the region in the vicinity of PPR 180°. The largest bays are in this region and as such the fundamental frequency of the panels or bays, are lower than at any other location on the bulkhead. The low fundamental frequency will generally correspond to a mode with the largest deformation at resonance and they should also be the easiest panels to excite. This scenario seems to fit well with observation, as when bulkhead web cracks are observed the tendency is for them to be located in the vicinity of radial 180°.

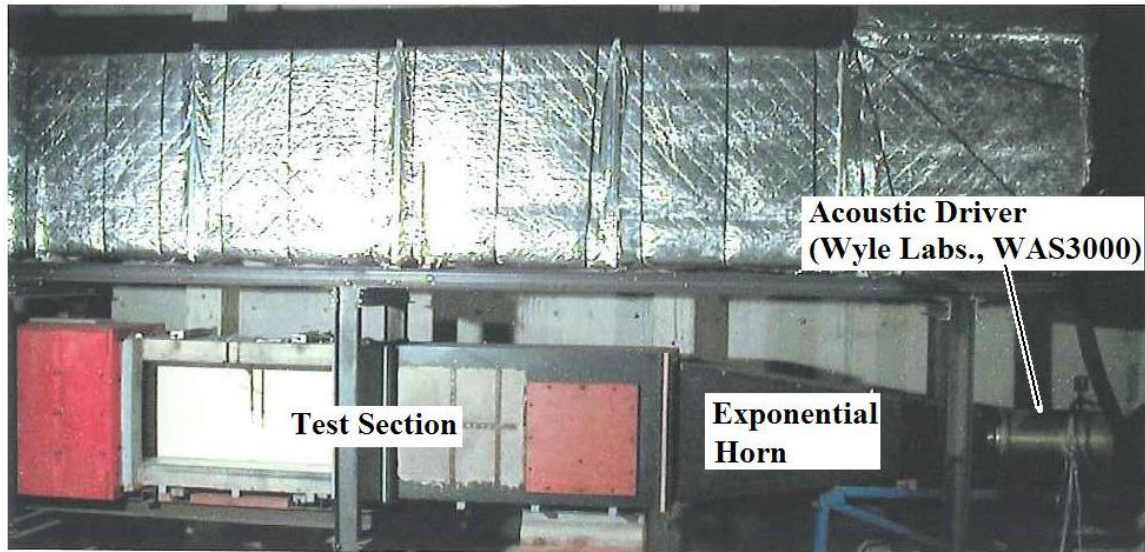


Figure 5 - PWT at the University of Southampton, England³.

3.1.1 Progressive wave tube test data

The specimen was first exposed to a sine sweep in the PWT to determine the predominant response frequencies (Figure 6). It was subsequently exposed to broad band acoustic loading; starting at a relatively low level and gradually increasing the sound pressure level (SPL). The test specimen had been instrumented with strain gauges and accelerometers. The data generated at the various SPLs is referred to as a linearity test. The linearity test was carried out at both room temperature and at elevated temperature (400°F). The results of these tests have been presented in Table 1 and Figure 7. The strain spectrum at 155dB has been included in Figure 8 for reference. It is interesting to note the similarity between the overall rms strain data generated at room temperature when compared to that generated at elevated temperature and also the non-linear behaviour beyond an overall sound pressure level of 155dB.

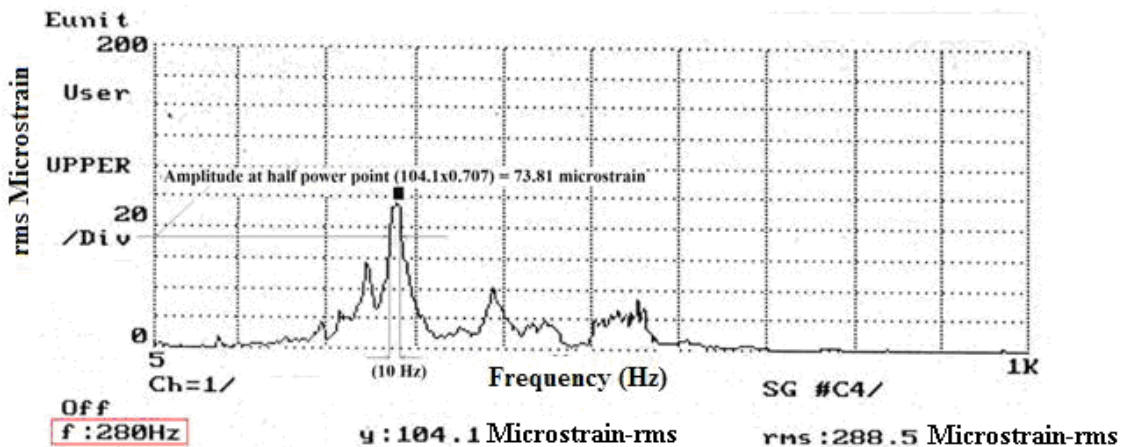


Figure 6 - Predominant response frequency of panel under swept sine wave excitation.

³ Photograph courtesy of Dr Paul Cunningham, Loughborough University, England [10].

OASPL (dB)	Room Temperature Results ($\mu\epsilon$)				Elevated Temperature Results ($\mu\epsilon$)			
	RT-1	RT-2	RT-3	RT-4	ET-1	ET-2	ET-3	ET-4
140	76.8	72.07	68.21	65.88	76.23	60.03	57.33	81.59
145	111.1	120.4	128.5	121	137.4	124.5	120.3	137
150	195.6	209.3	209.2	195.3	196.7	204	209.1	212.6
155	303.9	298.1	292.1	295.8	311.1	318.3	309.7	322.1

Table 1 - Linearity Test Results (Strain Gauge Results at centre of panel - ϵ_x)

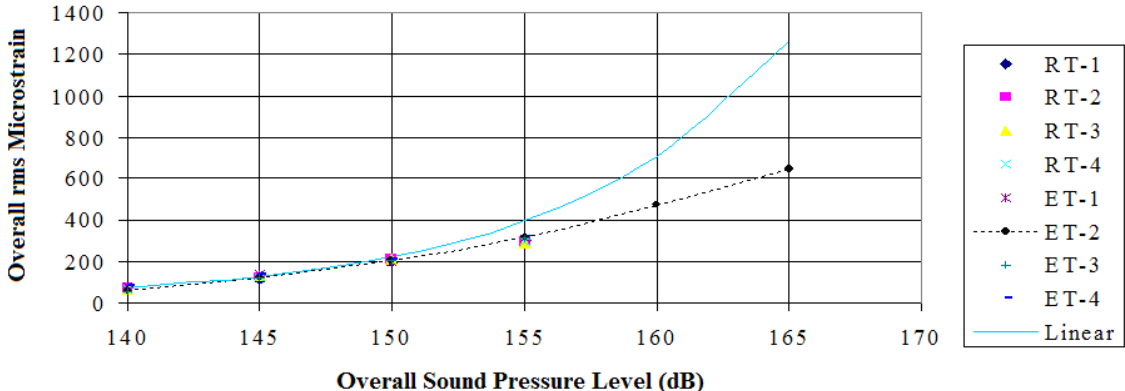


Figure 7 – Linearity test results (Titanium 3-bay bulkhead test specimen) along with the predicted response based on linear extrapolation of the initial response at 140dB⁴.

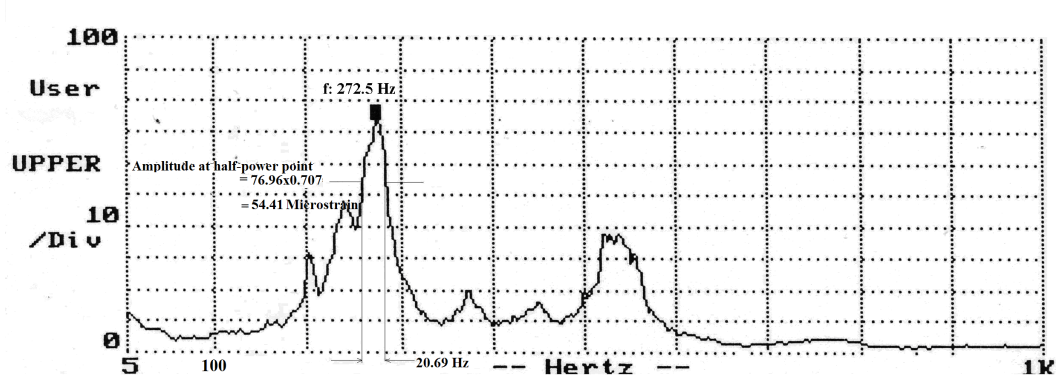


Figure 8 - Measured strain response at centre of a 3-bay panel array due to an OASPL of 155dB (600Hz BW) – Progressive Wave Tube test.

3.2 Flight test data

A strain gauge signal (measuring in the centre of the web bay in the circumferential direction i.e. normal to the stiffener), has been shown in Figure 9 for reference. For commercial reasons the absolute values of the strain gauge response have been omitted from Figure 9. Similarly, the measured sound pressure levels cannot be disclosed. Good coherence was demonstrated between the strain gauges and the SPL's measured adjacent to the fan. The SPL's were found to exceed the specification for the nacelle and the argument was made that in comparison with

⁴ SPL= $20 \log \left(\frac{P_{rms}}{P_{ref}} \right)$ [12], where $P_{ref}=20\mu\text{Pa}$. The stress or strain, is a function of the rms pressure (P_{rms}). A 6dB increase in SPL results in a doubling of the rms pressure, which in turn, results in a doubling of the rms stress (or strain).

the endurance demonstrated in the PWT test that had the engine SPL's been within the specification for the nacelle, the resulting strain levels would reduce to a level at which fatigue failure would not occur within the life of the aircraft.

Figure 9 shows the predominant response frequency is approximately 250Hz. This is reasonably close to the 270Hz – 280Hz of the predominant response frequency identified in the PWT test and shows that the use of the abbreviated bulkhead segment for the progressive wave tube test was acceptable in terms of capturing the dynamic behaviour of the structure despite the artificial boundary constraints necessary to constrain the PWT test specimen.

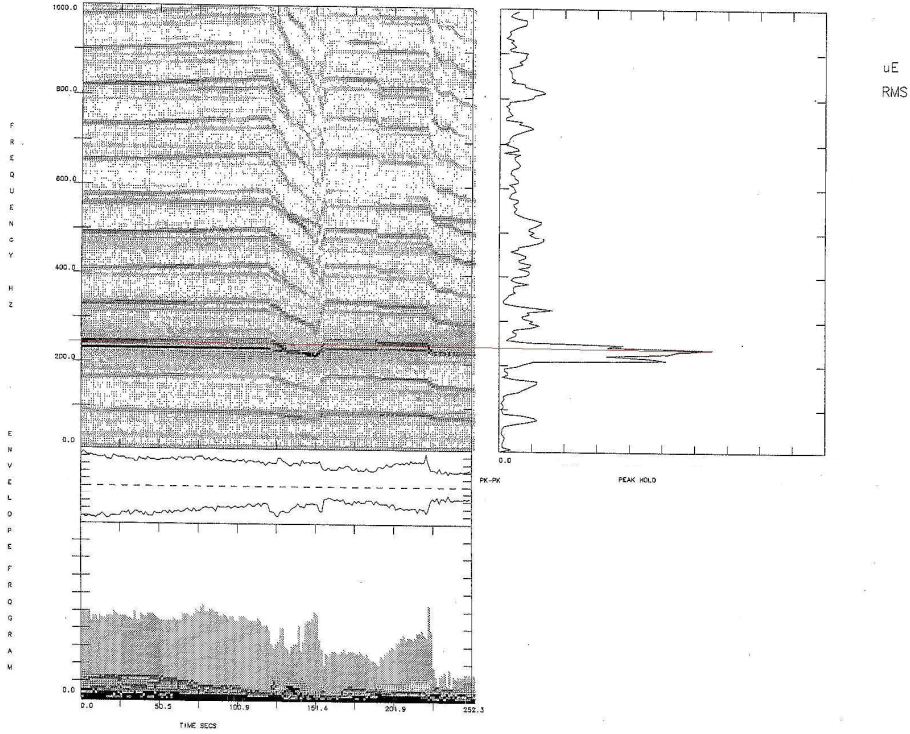


Figure 9 – Strain gauge response on bulkhead (flight test measurement).

4. RESPONSE PREDICTION

A finite element model representing the PWT segment of the bulkhead was generated in parallel with the test activity. To verify the fundamental frequency obtained from the FE model, textbook solutions [13] for a plate were used to estimate the fundamental frequency of a rectangular plate with idealised boundary conditions as per equation (1).

$$f_{ij} = \frac{\lambda_{ij}^2}{2\pi a^2} \left[\frac{Eh^3}{12\gamma(1-\nu^2)} \right]^{0.5} \quad (1)$$

$$\begin{aligned}
 h &= 0.71\text{mm (0.028")} \\
 a &= 0.19\text{m (7.59")} \\
 E &= 110.32 \text{ GPa (16x10}^6 \text{ lbf/in}^3\text{)} \\
 \rho &= 4438 \text{ kg/m}^3 \text{ (0.16 lbf/in}^3\text{)} \\
 \gamma &= \rho h = 3.15 \text{ kg/m}^2 \text{ (1.16x10}^{-5} \text{ lb(mass)/in}^2\text{)} \\
 \nu &= 0.3
 \end{aligned}$$

The frequency parameter λ is given in Blevins [13] for specific panel aspect ratios for the particular boundary condition and mode order of the plate. Generally one attempts to bound a problem by considering the boundary conditions to lie somewhere between all edges simply

supported and all edges fully fixed. The table below (Table 2) sets out the frequency parameters for the fundamental mode for three boundary conditions; all edges simply supported (S-S-S-S), all edges fixed (C-C-C-C) and one where the long edges of the panel (those parallel to the stiffeners) are fixed while the short edges of the panel (those parallel to the boundary angles) are simply supported i.e. S-C-S-C. Frequency parameters for the exact aspect ratio of 1.45 were not available and linear interpolation was used to establish the required values for the fundamental mode for each boundary condition being considered.

Boundary Condition =	SSSS	SCSC	CCCC
$\lambda_{1,1}$ for aspect ratio of 1.0 =	19.74	28.95	35.99
$\lambda_{1,1}$ for aspect ratio of 1.5 =	32.08	56.35	60.77
Interpolated $\lambda_{1,1}$ for aspect ratio of 1.45 =	48.35	93.09	96.63
Fundamental Frequency (Hz) =	169.33	326.02	338.44

Table 2 – Fundamental frequency for various boundary conditions (titanium plate 0.13m x 0.19m x 7.1×10^4 m).

Experience has shown that bulkheads of similar construction and configuration have boundary conditions approaching the S-C-S-C condition. However, the calculations show that the fundamental frequency is indeed bounded by the extreme conditions of all edges free and all edges fully fixed, and with regard to the FE model (Figure 10), at 227.24Hz, is approximately half-way between the condition with all edges simply supported and that of S-C-S-C.

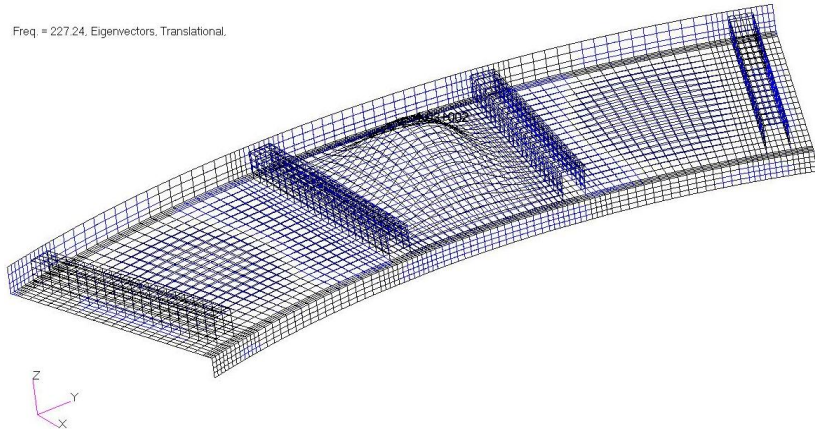


Figure 10 – FEM of 3-bay PWT specimen; fundamental mode of centre bay.

The response to acoustic loading was conducted using the traditional Miles equation with Blevins' modification for a joint acceptance of unity [5]. For an overall sound pressure level (OASPL) of 155dB, the stress at the centre of the mid bay was 26.13 MPa, which expressed as a strain equated to approximately $237\mu\varepsilon_{rms}$.

4.1 Dynamic stiffness method

The concept of the dynamic stiffness method (DSM) is to solve the differential equation of motion exactly, thus a single element can be used to represent a structural component without compromising accuracy. This is in contrast with the finite element method [14], where an

element is characterised by a shape function and the ability to represent a deformed shape is a function of the order of the shape function and the number of elements used.

There is a disadvantage with the DSM however in that an exact solution for the differential equation of motion is only generally available for a one dimensional structural element. Plates and shells can be analysed if it is assumed that two opposing edges are simply supported [15, 16, 17].⁵ In this application, a dynamic stiffness element based on the flat rectangular plate (Figure 11) described by Langley [15] has been used.

In the longitudinal direction x extends from zero to L and in the transverse direction y extends from zero to b .

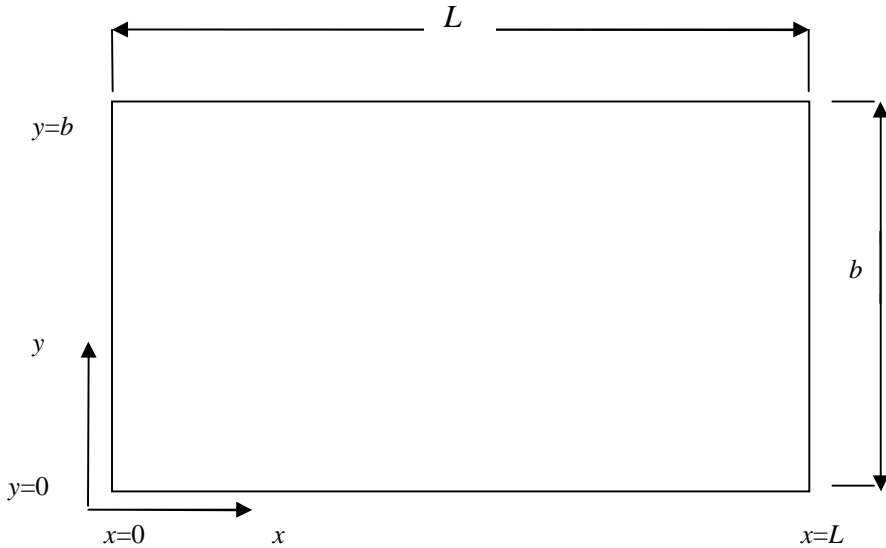


Figure 11 - Plate element configuration.

The differential equation describing the deflection (w) of a plate under a normal pressure q in terms of the plate bending stiffness⁶ D , the in plane pre-stresses N_x , N_y , the in-plane shear stress, N_{xy} and the body forces X and Y , was given by Timoshenko [18] as equation (2)⁷;

$$\frac{\partial^4 w}{\partial x^4} + 2 \frac{\partial^4 w}{\partial x^2 \partial y^2} + \frac{\partial^4 w}{\partial y^4} = \frac{1}{D} \left(q + N_x \frac{\partial^2 w}{\partial x^2} + N_y \frac{\partial^2 w}{\partial y^2} + 2N_{xy} \frac{\partial^2 w}{\partial x \partial y} - X \frac{\partial w}{\partial x} - Y \frac{\partial w}{\partial y} \right) \quad (2)$$

The Laplace operator (∇^2)⁸ was used to simplify equation (2) as follows;

$$D \nabla^4 w = q + N_x \frac{\partial^2 w}{\partial x^2} + N_y \frac{\partial^2 w}{\partial y^2} + 2N_{xy} \frac{\partial^2 w}{\partial x \partial y} - X \frac{\partial w}{\partial x} - Y \frac{\partial w}{\partial y} \quad (3)$$

Equation (3) can be simplified further by neglecting the in plane shear stress and tangential forces, i.e.

⁵ A solution is also available for when two opposing edges have sliding supports however, this is not a configuration generally encountered with the types of construction being considered in this application.

⁶ For an isotropic plate, the plate bending stiffness D is a function of Young's modulus E , plate thickness h and

Poisson's ratio ν and is defined as $D = \frac{Eh^3}{12(1-\nu)}$.

⁷ See Timoshenko [18], chapter 12 of the second edition.

⁸ $\nabla^2 = \frac{\partial^2}{\partial x^2} + \frac{\partial^2}{\partial y^2}$, $\nabla^4 = \frac{\partial^4}{\partial x^4} + 2 \frac{\partial^4}{\partial x^2 \partial y^2} + \frac{\partial^4}{\partial y^4}$

$$D\nabla^4 w = q + N_x \frac{\partial^2 w}{\partial x^2} + N_y \frac{\partial^2 w}{\partial y^2} \quad (4)$$

Re-arranging the above expression and including an inertia term for dynamic analysis yields the following equation of motion, where rho (ρ) is the mass density and h is the plate thickness;

$$q = D\nabla^4 w - N_x \frac{\partial^2 w}{\partial x^2} - N_y \frac{\partial^2 w}{\partial y^2} + \rho h \frac{d^2 w}{dt^2} \quad (5)$$

The out of plane displacement w is a function of the spatial co-ordinates x and y and time t . Assuming a harmonic variation in time for both the loading q and with a further imposition that the edges along $y=0$ and $y=b$ are simply supported, then the displacement response w becomes a function of the mode order⁹ m , across the width b , i.e.

$$w(x, y, t) = \sum_m X_m(x) \sin\left(\frac{m\pi y}{b}\right) e^{j\omega t} \quad (6)$$

Using equation (6) and by making the relevant substitutions for w , equation (5) after multiplying both sides by $\sin\left(\frac{n\pi y}{b}\right)$ and then integrating with respect to y from 0 to b can be expressed as follows¹⁰:

$$\int_0^b q \sin\left(\frac{n\pi y}{b}\right) dy = e^{j\omega t} \sum_m \left[\int_0^b \sin\left(\frac{n\pi y}{b}\right) \sin\left(\frac{m\pi y}{b}\right) dy \right] \quad (7)$$

Note, the integration term on the right hand side is zero for values of n not equal to m and $0.5b$ for values of n which are equal to m i.e.

$$\frac{2}{b} \int_0^b q \sin\left(\frac{n\pi y}{b}\right) dy = \begin{bmatrix} DX_n^{iv}(x) - (2Dk_n^2 + N_x)X_n''(x) \\ + (Dk_n^4 + N_y k_n^2 - \rho h \omega^2)X_n(x) \end{bmatrix} \quad (8)$$

The pressure q represents a pressure normal to the surface of the plate. To describe a propagating harmonic plane acoustic wave q is a function of x , y and t and can be expressed in exponential form [15] as

$$q(x, y, t) = e^{(-j\mu_1 x - j\mu_2 y + j\omega t)} \quad (9)$$

The quantities μ_1 and μ_2 are the real wave numbers of the propagating pressure loading travelling with speeds $\frac{\omega}{\mu_1}$ and $\frac{\omega}{\mu_2}$ in the x and y directions respectively. For a simplistic case one can assume μ_1 and μ_2 are zero, which represents a uniform harmonic pressure, similar to the basic assumption made in the Miles equation [1].

⁹ Following the notation used by Langley [15]

¹⁰ Where the missing terms within the parenthesis are given as;

$$\left[D \frac{\partial^4 X_m(x)}{\partial x^4} - 2D \frac{\partial^2 X_m(x)}{\partial x^2} \left(\frac{m\pi}{b} \right)^2 + DX_m(x) \left(\frac{m\pi}{b} \right)^4 - N_x \frac{\partial^2 X_m(x)}{\partial x^2} + N_y X_m(x) \left(\frac{m\pi}{b} \right)^2 - \rho h X_m(x) \omega^2 \right]$$

The solution of the differential equation of motion (equation (8)) involves solving the complementary function and the particular integral. The complementary function relates the forces and displacements in the absence of any distributed loading however forces at the element boundary can be accommodated.

The process leads to expressing the displacements and rotations with respect to the wave amplitudes by a square matrix P_1 , while the forces and moments are related to the wave amplitudes by another square matrix P_2 . Note that the notation used here and in the plate element described in section 2.2 which follows, is similar to that of Langley [15].

The dynamic stiffness matrix (Q) is subsequently defined by equation (10).

$$Q = P_2 P_1^{-1} \quad (10)$$

The PWT test panel of Figure 4, comprising three panel bays, was represented by eight dynamic stiffness elements (Figure 12). The elements were based on rectangular plate elements using the procedure described by Langley [15]. The hat section stiffeners were also modelled as plate elements where the thickness of the plate was calculated on the basis of an equivalent bending stiffness for an effective width of stiffener (Figure 13, Table 3).

The mid bay was represented by two elements in order to facilitate the application of point loads if required. The mid bay is the panel of greatest interest. The bays on either side were fastened into the test fixture (in the actual test specimen) and as stated previously, the mid bay is the only bay of the test panel which has the most realistic boundary conditions when comparing the test specimen with an actual bulkhead panel array.

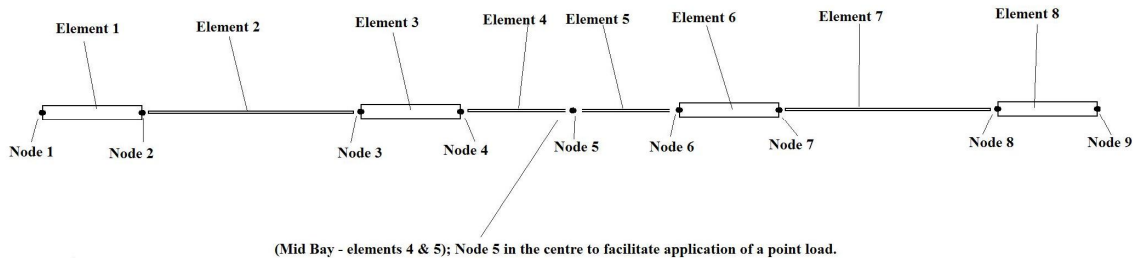


Figure 12 – DSM representation of a 3-bay bulkhead PWT specimen.

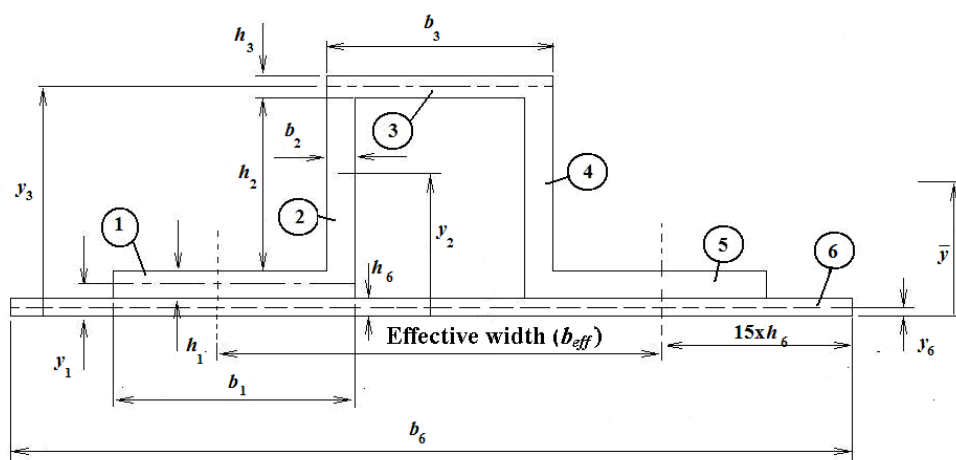


Figure 13 – “Hat” section stiffener configuration.

Item #	Width - b (m)	Height h (m)	Distance to Centroid - y (m)	Cross Sectional Area - A (m^2)	Ay - (m^3)	Ay^2 - (m^4)	2 nd Moment of Area about centroid - I (m^4)
1	25.40	1.02	1.22	25.81	31.46	38.36	2.22
2	1.02	23.37	13.41	23.74	318.41	4270.22	1080.38
3	25.40	1.02	25.60	25.81	660.73	16916.71	2.22
4	1.02	23.37	13.41	23.74	318.41	4270.22	1080.38
5	25.40	1.02	1.22	25.81	31.46	38.36	2.22
6	48.77	0.71	0.36	34.68	12.33	4.39	1.46
$\Sigma =$				159.59	1372.80	25538.26	2168.88

Table 3 – Second moment of area calculation (tabular method).

$$\begin{aligned}
 \bar{y} &= \frac{\Sigma Ay}{\Sigma A} \\
 &= \frac{1378.2}{159.59} \\
 &= 8.60 \text{mm}
 \end{aligned} \tag{11}$$

2nd Moment of Area about neutral axis;

$$\begin{aligned}
 I_{na} &= \sum I + \sum Ay^2 - \sum A \times \bar{y}^2 \\
 &= 2168.88 + 25538.26 - (159.59)8.60^2 \\
 &= 15898.01 \text{ mm}^4
 \end{aligned} \tag{12}$$

This can subsequently be used to determine the thickness of a rectangular section (flat plate) of a given width. One could choose a width equal to that of the width of stiffener plus the strip of effective skin (the skin being the bulkhead web in this application). Another alternative is to choose the width between the fasteners which attach the stiffener to the web.

For comparison with single panel results the width of each panel bay was based on the average width between the fastener rows attaching the stiffeners to the web. It would seem prudent therefore to base the equivalent stiffener width on the distance between the fasteners.

Referring to Figure 13, and knowing that the fastener line is 12.7mm from the free edge of the stiffener, the distance between the fasteners was given as;

$$\begin{aligned}
 \text{Effective width;} \quad b_{eff} &= [2((b_1 - b_2) - 12.7)] + b_3 \\
 &= 48.77 \text{ mm}
 \end{aligned} \tag{13}$$

The second moment of area of a rectangular section was given as

$$I = \frac{bd^3}{12} \tag{14}$$

Rearranging this equation to give the thickness term (d) in terms of the other parameters;

$$d = \sqrt[3]{\frac{12I}{b}} \tag{15}$$

$$\begin{aligned}
&= \sqrt[3]{\frac{12 \times 15898.01}{48.77}} \\
&= 15.76 \text{ mm}
\end{aligned}$$

Therefore the stiffener can be replaced by a plate made from the same material and of rectangular cross section with the dimensions 48.77mm wide by 15.76mm thick. Note that the density of the equivalent section will need to be reduced – a solid block of material $48.77 \times 15.76 \text{ mm}^2$ (768.62 mm²) is much greater than the area of the hat section stiffener plus the local piece of bulkhead web to which the stiffener is attached (159.59 mm²). Therefore for the same given length the density of the equivalent stiffener would have to reduce by a factor of 4.8 in order to have the same mass and stiffness as the actual components.

The dynamic stiffness matrices for each element were combined to give an assembled dynamic stiffness matrix G_n . The nodal displacements $\{z_n\}$ were obtained by multiplying the assembled force vector (g_n) by the inverse of the assembled dynamic stiffness matrix, as shown in equation (15).

$$\{z_n\} = [G_n]^{-1} \{g_n\} \quad (16)$$

The assembly and solution of the various matrices was achieved using standard finite element techniques [14]. Having calculated the nodal displacements it was then possible to calculate the displacement at any point in the various plate elements. Expressions for strain in the plate were developed [11] based on second order derivatives of displacement.

At a frequency of approximately 250Hz, the acoustic half wavelength is 0.7m (27"). The bays were less than 0.15m (6") wide and as such the applied loading was modelled as a uniform pressure.

Acoustic fatigue is essentially a random vibration phenomenon and the random response was determined by multiplying the power spectral density of the acoustic loading by the square of the magnitude of the plate transfer function to give the power spectral density response of the plate. Integrating the output PSD with respect to frequency gave the mean square value. The evaluation of the root mean square (rms) and overall rms values was subsequently trivial.

Two boundary constraint conditions were considered. In the first, the DSM model had simply supported edge conditions at node 1 and node 9 (Figure 12). For the second condition, fixed edge conditions were applied at nodes 1 and 9 (Figure 12). The applied loading was 155 dB and the bandwidth was based on the test exposure which had a flat spectrum between 100 & 700 Hz (i.e. 600 Hz bandwidth). The results along with those for a single plate have been presented in Table 4. The analysis assumed an equivalent critical viscous damping ratio of 1.7%. This was applied in the DSM as a complex Young's modulus term. The value of equivalent critical viscous damping ratio of 1.7% compares favourably with the damping calculated using the half-power point technique [19] on the data in Figure 6.

The results using the DSM have been summarised in Table 4. For comparative purposes, a single plate or a single panel bay was modelled also. Broadly speaking, in terms of the three-bay model configurations the centre bay shows little difference in the overall strain levels between either fully fixed or simply supported boundary conditions. The single plate model, however, exhibits a much greater influence of boundary constraint as one might expect. However, when comparing the results between the single plate and the assembly of plate elements it is clear that the single panel when subject to the fully fixed edge condition along the edges, to which the stiffeners would attach, gave a result very similar to that when modelling the three bays.

Note that in relation to the results in Table 4, the x -direction relates to the circumferential direction of the bulkhead, while the y -direction is parallel to the axis of the stiffeners (i.e. in the radial sense of the bulkhead).

Configuration	Displacement (mm)	Overall rms Strain ($\mu\epsilon_{rms}$)	
		Strain-x	Strain-y
3-Bay (S-S-S-S)	0.99	364.59	255.39
3-Bay (S-C-S-C)	0.92	363.03	252.03
Single Plate (S-S-S-S)	1.9	394.44	289.44
Single Plate (S-C-S-C)	0.92	325.69	251.68

Table 4 – Results of DSM modelling of PWT specimen (Mid bay response; 155dB OASPL).

The modelling suggests the stiffeners bounding the centre bay impose fixed edge conditions given that the fixed edge condition of the single panel was very similar to the results from the three-bay model with either edge condition. This provides an interesting result in itself and suggests that an effective stiffener is one which creates a fixed edge condition. The process has three steps;

1. Model a single panel using the simply supported – fixed – simply supported – fixed edge conditions.
2. Model a 3-bay panel and vary the thickness of the elements representing the stiffeners (elements 1, 3, 6 & 7 in the example used above) until the response of the mid bay approaches that of the single panel model.
3. Knowing the desired effective thickness of the stiffener the actual stiffener dimensions can be extracted out from a spreadsheet as used in the above example to establish the stiffener second moment of area.

The stiffener performance is enhanced when the skin thickness is low. In the example referred to above, the stiffener was formed from a sheet thickness of 1.02mm whereas the skin thickness of the web was 0.71mm (a ratio of 1.44) and it is easier to introduce a fixed edge condition with a stiffener when the skin thickness is much lower than the stiffener wall thickness in combination with the web running continuously under the stiffeners (unlike the attachment at the inner and outer boundary angles, where the skin terminates).

The strain response using the DSM at the centre of bay-2 for the 3-bay configuration has been shown superimposed on that relating to the single bay model in Figure 14, which demonstrates how effective the stiffeners (on this particular bulkhead configuration) are in constraining the edge of the panel and also how effective the DSM models have been in capturing this behaviour when compared with the measured data shown in Figure 8.

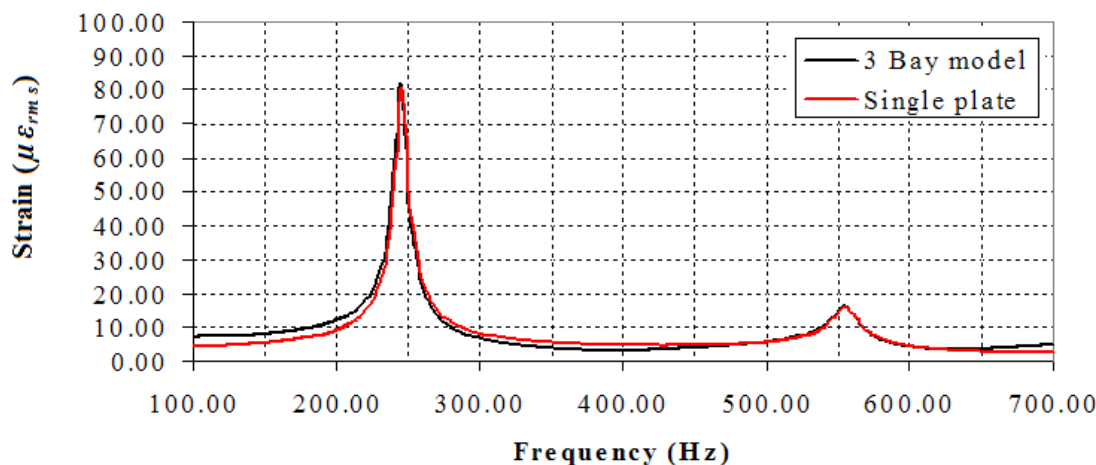


Figure 14 – Strain response at centre of a 3-bay panel array along with the strain response at centre of a single panel, due to an OASPL of 155dB (600Hz BW); Simply supported – Clamped - Simply supported – Clamped boundary conditions.

With regard to the spectral content, the DSM methods both have a peak in the frequency response spectrum at approximately 244.5 Hz and 556 Hz for the secondary peak (555 Hz for the 3-bay model). The PWT panel (Figure 4), which the DSM was attempting to model had a predominant response frequency of 272.5 Hz with a secondary peak at approximately 540 Hz as shown in (Figure 8). The difference in frequency was approximately 10%. Comparing both the PWT results and the DSM prediction, with measurements made on an actual bulkhead used in flight testing (Figure 9), only the fundamental mode appears to be common.

In terms of strain response for the 155dB OASPL, the overall rms strain for the single bay configuration with S-C-S-C boundary conditions was of the order of $325\mu\varepsilon_{rms}$ while for the actual PWT panel showed an overall strain of $298.1\mu\varepsilon_{rms}$. The response at the predominant response frequencies was approximately $80\mu\varepsilon_{rms}$ for both DSM configurations while the actual PWT specimen showed $76.96\mu\varepsilon_{rms}$. In terms of both the response at the predominant frequency and the overall strain the DSM was in excellent agreement with the measured response. Although there is a slight over-prediction in the rms response when using the DSM, this is advantageous for a design tool. It should be emphasised that the DSM formulation used in this example was linear as in its assumptions the excitation and response are harmonic. In-plane loads were not included although as shown in equation (2) in plane loads could have been retained. Bercin and Langley [16], have formulated a dynamic stiffness element which includes the effect of in-plane loading and this is something which could be explored here to establish if the non-linear behaviour observed in the PWT test at higher sound pressure levels could be replicated.

5. CONCLUSION

An overview of fatigue problems encountered with nacelle bulkheads has been provided. Details of how such problems can be addressed and some of the data generated as part of the in-service failure investigation has been summarised for reference. Endurance testing has highlighted the highly non-linear behaviour at high sound pressure levels but has also shown, that at normal operating SPLs, a linear analysis is sufficient to analyse this particular component.

Finite element techniques have been discussed and the use of the dynamic stiffness method has also been summarised. The dynamic stiffness method provided a good overall assessment of the bulkhead response (within the linear range) when compared with PWT test data generated on a representative bulkhead test specimen, despite some of the simplifications applied to the modelling assumptions; such as the way the stiffeners were represented and also modelling the curved bulkhead segment with rectangular plate elements. The use of the DSM is much more computationally efficient than the finite element method, although the DSM does have certain limitations. The finite element model gives a more general overview and allows a good visual representation to be observed of the entire model behaviour. It is important though to bear in mind that this particular finite element model had a total of 4513 nodes and 5184 elements in comparison with the nine nodes and eight elements of the (largest) DSM model used.

Suggestions as to how the DSM could be used to quickly optimise a basic bulkhead configuration have been presented. Having obtained a suitable configuration using the DSM, more time could then be devoted to a detailed design specific finite element modeling of the optimised configuration.

REFERENCES

- [1] J.W. Miles, On Structural fatigue under random loading, *Journal of Aeronautical Sciences*, (21), p753:762, 1954.
- [2] F.F. Rudder, H.E. Plumlee, Jr., *Sonic Fatigue Design Guide For Military Aircraft*, AFFDL-TR-75-112, Air Force Flight Dynamics Laboratory, Wright Patterson Air Force Base, Ohio, USA, 1975.
- [3] Engineering Sciences Data Unit (ESDU) International plc, 27 Corsham Street, London, N1 6UA, (Series on Vibration and Acoustic Fatigue).
- [4] A. Powell, A., On the failure of structures due to vibrations excited by random pressure fields," *Journal of the Acoustical Society of America*, Vol. 30, No. 12, p1130-1135, 1958.
- [5] R.D. Blevins, An approximate method for sonic fatigue analysis of plates and shells, *Journal of Sound and Vibration*, 129(1):p51-71, 1989.
- [6] B.L. Clarkson, *Review of Sonic Fatigue Technology*, NASA Contractor Report 4587, National Aeronautics and Space Administration, Langley Research Center, Hampton, Virginia, USA, 1994.
- [7] I. Holehouse, Sonic fatigue of aircraft structures due to jet engine fan noise, *Journal of Sound and Vibration*, 17(3), p287-298, 1971.
- [8] J. Soovere, J., Correlation of sonic fatigue failures in large fan engine ducts with simplified theory, AGARD CP113 (*Symposium on Acoustic Fatigue, Toulouse, France*), p11-1 – 11-13, 1972.
- [9] D.M.A. Millar, The behaviour of light weight honeycomb sandwich panels under acoustic loading, N.S. Ferguson, H.F. Wolfe, C. Mei eds. *Proceedings of the 6th International Conference; Structural Dynamics – Recent Advances, Institute of Sound and Vibration Research (ISVR), Southampton, England*, 1997.
- [10] P.R. Cunningham, *Response Prediction of Acoustically-Excited Composite Honeycomb Sandwich Structures with Double Curvature*, PhD Thesis, University of Southampton, England, 2001.
- [11] D.M.A. Millar, *The Application of the Dynamic Stiffness Method for the Acoustic Fatigue Analysis of Aircraft Engine Nacelle Structures*, PhD Thesis, University of Southampton, England, 2012.
- [12] L.E. Kinsler, A.R. Frey, A.B. Coppens, J.V. Sanders, *Fundamentals of Acoustics*, 3rd Ed., John Wiley and Sons, New York, 1984.
- [13] R.D. Blevins, *Formulas for Natural Frequency and Mode Shape*, Robert E. Krieger Pubs., Co., Inc., Malabar, Florida, USA, (reprint Ed.), 1984.
- [14] O.C. Zienkiewicz, *The Finite Element Method in Engineering Science*, (Third Edition), McGraw-Hill, London, 1977.
- [15] R.S. Langley, Application of the dynamic stiffness method to the free and forced vibrations of aircraft panels, *Journal of Sound and Vibration*, 135(2), p319-331, 1989.
- [16] A.N. Bercin, R.S. Langley, Application of the Dynamic Stiffness Technique to The In-Plane Vibrations of Plate Structures, *Computers & Structures*, Vol. 59, No. 5, p869-875, 1996.
- [17] R.S. Langley, A dynamic stiffness technique for the vibration analysis of stiffened shell structures, *Journal of Sound and Vibration*, 156(3), p521-540, 1992.
- [18] S.P. Timoshenko, S., Woinowsky-Krieger, *Theory of Plates and Shells*, Second Edition, McGraw-Hill Book Company, 1959.
- [19] W.T. Thomson, *Theory of Vibration with Applications*, 3rd Edition, Unwin Hyman Ltd., London, 1988.